Dipole switching dynamics in P(VDF-TrFE) film revealed by in-situ polarization switching and infrared spectroscopy measurements with high-time resolution

Uneda, Kohki
Horike, Shohei
Koshiba, Yasuko
Ishida, Kenji

(Citation)
Polymer,249:124822

(Issue Date)
2022-05-17

(Resource Type)
journal article

(Version)
Version of Record

Polymer 249 (2022) 124822

Contents lists available at ScienceDirect

Polymer

journal homepage: www.elsevier.com/locate/polymer

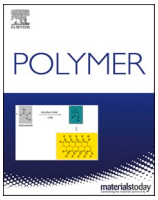

Dipole switching dynamics in P(VDF-TrFE) film revealed by in-situ polarization switching and infrared spectroscopy measurements with high-time resolution

Kohki Uneda [a], Shohei Horike [a,b,c], Yasuko Koshiba [a,b], Kenji Ishida [a,b,*]

[a] Department of Chemical Science and Engineering, Graduate School of Engineering, Kobe University, 1-1 Rokkodai-cho, Kobe, 657-8501, Japan
[b] Research Center for Membrane and Film Technology, Kobe University, 1-1 Rokkodai-cho, Kobe, 657-8501, Japan
[c] PRESTO, Japan Science and Technology Agency, Kawaguchi, 332-0012, Japan

ARTICLE INFO

Keywords:
P(VDF-TrFE)
Dipole switching dynamics
High-time resolution infrared spectroscopy

ABSTRACT

Although P(VDF-TrFE) is an important ferroelectric material, its polarization switching details, especially at the nucleation site of the polarized domain, are unknown. Herein, a setup combining a ferroelectricity evaluation system and a Fourier-transform infrared spectrometer with a 70 ms time resolution was developed to simultaneously monitor polarization-switching current and absorption changes associated with the molecular chain rotation of P(VDF-TrFE) under an electric field. Time variations of absorbance associated with CF_2 symmetric vibration in response to the applied electric field served as an indicator of dipole rotation. The onsets and peaks of the polarization-switching current, which appeared before the dynamic molecular orientation, changed across the material. The complementary characterization revealed that the P(VDF-TrFE) polarized domain first nucleates at the interface and grows toward the inner side of film to achieve a completely polarized state of the film.

1. Introduction

Ferroelectrics are dielectric materials with nonvolatile electric dipoles that can be preserved in response to an external electric field [1]. Piezoelectric and pyroelectric properties form a subset of the ferroelectric effect [2], and class of materials that exhibit such properties has a wide range of applications such as nonvolatile memories [3], capacitors [4], infrared sensors [5], and sonars [6]. To date, $PbTiO_3$ (PZT), a state-of-the-art ferroelectric material with a large remanent polarization (600–700 mC m^{-2}) has been used in commercial devices [7]. For human and environmental safety reasons, the use of lead-containing materials should be avoided. PZT is currently excluded from the scope of the RoHS directive because it is difficult to replace PZT with other materials owing to its high performance. To achieve environmentally friendly ferroelectric materials, there has been an increasing number of studies on organic ferroelectric families [8–12]. Of these, vinylidene fluoride ($-CH_2CF_2-$; VDF)-based polymers have been shown to be a promising alternative owing to their nontoxicity. Their excellent flexibility and lightweight properties also suggest new technologically useful applications such as motion-to-electricity conversion devices for future energy harvesting [13–15].

The electric dipole of VDF derivatives (~2.1 D per monomer unit), responsible for the ferroelectric effect, originates from the difference in the electronegativities between the hydrogen and fluorine atoms bonded to the polymer chain. VDF-based polymers and oligomers typically have five crystalline phases with different conformations: all-*trans* conformations for the β-phase, TGTG′ conformations for the α- and δ-phases, and T_3GT_3G' conformations for the γ- and ε-phases [16–19]. The β-phase crystal exhibits the largest ferroelectricity, while the α crystal exhibits only paraelectricity, and the ferroelectricity of the γ crystal is at most ~64% of that of the β-phase structure. In PVDF (homopolymer of VDF), the paraelectric α-phase is the most stable crystal structure because of the steric hindrance between the nearby fluorine atoms in the all-*trans* conformation of the β-phase crystal. To obtain the β-phase crystal structure, the PVDF film must usually be subjected to stretching and/or a massive electric field [20,21]. In contrast, a copolymer of VDF and trifluoroethylene (TrFE), P(VDF-TrFE), can form a β-phase-rich crystalline film by a facile wet process (*e.g.*, spin coating) and an annealing treatment at low temperature (~130 °C) [22,23], with which it shows relatively large remanent polarizations (up to 70 mC m^{-2}) [24], pyroelectric

* Corresponding author. Department of Chemical Science and Engineering, Graduate School of Engineering, Kobe University, 1-1 Rokkodai-cho, Kobe, 657-8501, Japan.
E-mail address: kishida@crystal.kobe-u.ac.jp (K. Ishida).

https://doi.org/10.1016/j.polymer.2022.124822
Received 9 February 2022; Received in revised form 1 April 2022; Accepted 4 April 2022
Available online 13 April 2022

coefficients (50 μC m^{-2} K^{-1}) [25], and piezoelectric constants (d_{33} = 20 p.m. V^{-1}) [26]. Fig. 1 shows the most investigated P(VDF-TrFE) phases: α, β, and γ-phases. It has been recognized that the α-phase crystal structure could become unstable owing to the steric hindrance between the hydrogen and fluorine atoms in the TGTG' conformation by introducing the TrFE units, making the β-phase crystal energetically favored [27]. With the aid of such processability, P(VDF-TrFE) has often been used to reveal the properties of VDF derivatives, such as molecular orientation [28], crystal structure [29], phase transition (the presence of a Curie point) [30], and polarization mechanisms [31].

From a physical chemistry point of view, the mechanism of polarization switching is one of the most important issues to be addressed because it directly reflects the interactions between the P(VDF-TrFE) electric field and P(VDF-TrFE)–electrode and intermolecular interactions between P(VDF-TrFE)–P(VDF-TrFE). The typical model of polarization switching in VDF polymers includes four steps [32,33]: (1) nucleation of a polarized region in response to the applied electric field, (2) formation of a domain by the growth of the nucleus in the direction of the electric field, (3) transversal growth of the domain across the material, and (4) domain coalescence. The propagation processes (2)–(3) were previously investigated using X-ray diffraction (XRD) [34]. It has been proposed that the polarized domain grows along with one 180° rotation or three 60° rotations. Regarding the nucleation step (1), the detailed polarization switching dynamics were recently investigated. It was proposed that the nucleation starts from a 90° rotation of the repeated VDF unit against the polymer chain (so-called "kink") in the initial switching process [35].

Despite such progress in unraveling the polarization switching mechanisms of VDF polymers [33], nucleation processes are still being studied with two plausible scenarios: (1) both the nucleation and growth of the domains occur randomly in the film, and (2) nucleation starts from the interface of the VDF polymer and electrodes because a higher electric field is applied to the interface compared to the film bulk. Whereas the first scenario is likely if the rate of nucleation were higher than that of the growth steps, the second situation would be plausible if the growth rate of the domain were higher than that of nucleation. To verify these nucleation mechanisms, detection of the molecular orientations and crystal structures of the VDF polymers *after* polarization by varying the amplitude of the electric field (*ex situ measurement*) is not sufficient.

Instead, we developed a setup for *simultaneous (in situ)* observations of polarization switching (electrical measurement) and structural analysis (fast-time-resolved FT-IR spectroscopy). By monitoring the molecular orientation changes throughout the polarization switching with high resolutions in frequency and time, and comparing them with the switching current behavior, we identified that the initial nucleation sites of P(VDF-TrFE) are at the interface of P(VDF-TrFE) and the electrode.

2. Experimental

2.1. Chemicals and device preparation

The materials used in this study are listed in Table S1 of Supporting Information (SI). A P(VDF-TrFE) sample with a molecular weight of 300,000 and molar compositional ratio of 75:25 VDF-to-TrFE units was used. For simultaneous electrical and spectroscopic measurements, we fabricated an Al/P(VDF-TrFE)/NiCr stacked device, schematically illustrated in Fig. 2. Infrared rays can pass through the top NiCr electrode [36] while being reflected by the bottom Al electrode; therefore, molecular vibrations in the P(VDF-TrFE) layer could be detected by the reflection absorption spectroscopy (RAS) technique while applying an electric field between the two electrodes. The bottom Al electrode (thickness: 100 nm) was vapor-deposited onto a quartz glass substrate of dimensions 20 mm × 20 mm. A solution of 10 wt% P(VDF-TrFE) in methylethylketone was then spin-coated onto the substrate at 2500 rpm for 30 s, followed by annealing at 130 °C for 1.5 h to promote crystallization. The obtained P(VF-TrFE) film had a thickness of ~1.2 μm. Finally, the top NiCr electrode was vapor-deposited to a thickness of 8 nm. The surface morphology of the P(VDF-TrFE) film did not change significantly, suggesting negligible damage caused by radiant heat during the NiCr deposition (for more details, see Fig. S1 in SI). Au leads were attached to both the top and bottom electrodes for wiring to the ferroelectricity evaluation setup.

2.2. Characterization

A schematic of the setup for the simultaneous measurement of molecular vibrations and polarization switching is shown in Fig. 2. Au leads attached to the electrode of the sample were connected to a ferroelectric evaluation system (FCE-1, Toyo). A 0.01 Hz triangular voltage was applied to the top NiCr electrode while the bottom Al electrode was grounded. The voltage was scanned as 0 → +120 → −120 → 0 V while monitoring the electric current flowing through the circuit. Here, the applied voltage of 120 V corresponds to the application of an electric field of 100 MV m^{-1} to the P(VDF-TrFE) layer. The Al/P(VDF-TrFE)/NiCr stacked device was set in the FT-IR measurement system (FT/IR-6600, JASCO). Fast time-resolved FT-IR measurements (rapid scanning) and electrical measurements were performed simultaneously. The time and wavenumber resolutions were 70 ms and 4 cm^{-1}, respectively.

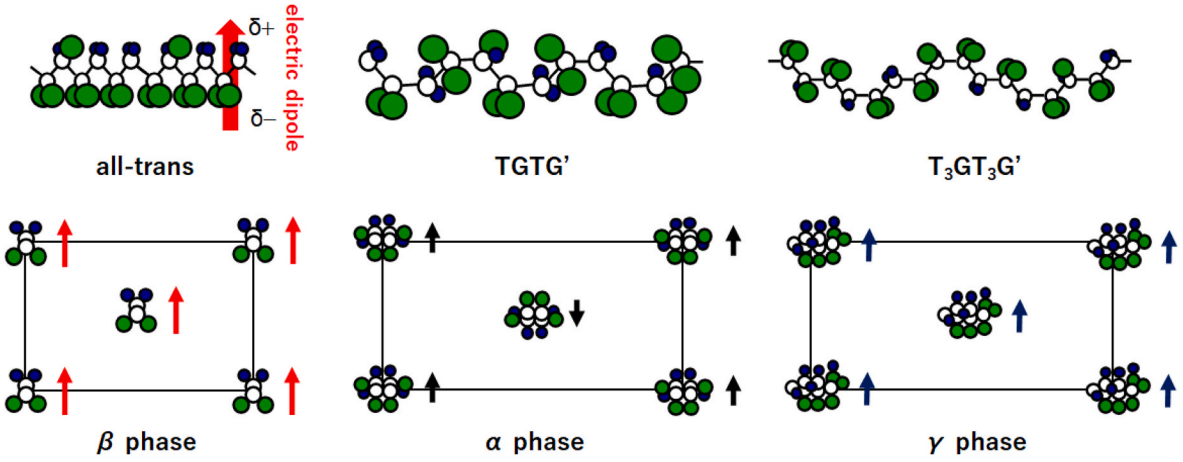

Fig. 1. Molecular conformations and crystal structures of P(VDF-TrFE). Blue, green, and white balls indicate hydrogen, fluorine, and carbon atoms, respectively. (For interpretation of the references to colour in this figure legend, the reader is referred to the Web version of this article.)

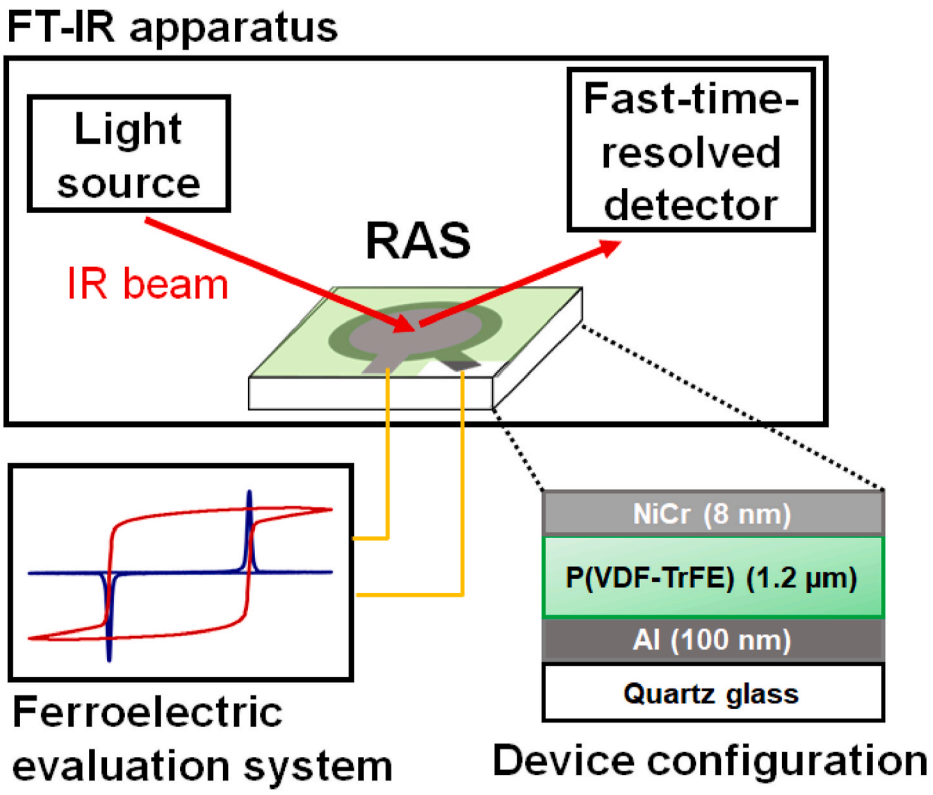

Fig. 2. Schematic of simultaneous measurement setup of polarization switching, FT-IR spectroscopy, and the device configuration.

3. Results and discussion

We evaluated the molecular vibrations of P(VDF-TrFE) using the RAS technique. In this technique, the applied infrared is absorbed when the transition moment of the molecular vibration is aligned in the out-of-plane direction of the film [37]. Because the poling treatment of P(VDF-TrFE) corresponds to inducing the out-of-plane orientation of the P(VDF-TrFE) electric dipoles, this spectroscopy technique can directly monitor ferroelectricity-related molecular orientation changes in response to an applied electric field. Typical RAS spectra of P(VDF-TrFE) films in the wavenumber ranges of 1150–1350 cm^{-1} and 820−920 cm^{-1} are shown in Fig. 3a and b, respectively, for both before and after poling treatments (for the spectra in the wider wavenumber range, see Fig. S2 and ESI). The detailed peak assignments are shown in Table 1. As shown in Fig. 3a, the distinctive peak at 1306 cm^{-1}, which corresponds to the CF_2 symmetric stretching vibration (ν_s (CF_2)) of the β-phase crystal [38], increased upon poling treatment. Meanwhile, the absorption peak at 893 cm^{-1} caused by the CF_2 asymmetric stretching vibration (ν_a (CF_2)) of the β-phase crystal decreased after poling, as shown in Fig. 3b. CF_2 groups should be oriented randomly in the P(VDF-TrFE) film before poling. After the poling treatment, the alignment of electric dipoles was induced in the out-of-plane direction of the

Table 1
Assignments of FT-IR spectrum of P(VDF-TrFE).

Wavenumber (cm^{-1})		Assignment
β phase	γ phase	
852		$\nu_s(CF_2)$, $\nu_s(CC)$
893		$\nu_a(CF_2)$, $r(CH_2)$, $r(CF_2)$
1075		$\nu_a(CF_2)$, $w(CH_2)$, $w(CF_2)$
	1125	$\nu_s(CF_2)$, $w(CH_2)$
1185		$\nu_a(CF_2)$, $r(CH_2)$, $r(CF_2)$
	1201	$\nu_a(CF_2)$
	1238	$\nu_a(CF_2)$, $r(CH_2)$
1306		$\nu_s(CF_2)$, $r(CH_2)$, $r(CF_2)$
	1330	$\delta(CH_2)$, $w(CH_2)$
1400		$\nu_a(CC)$, $w(CH_2)$
1430		$\delta(CF_2)$

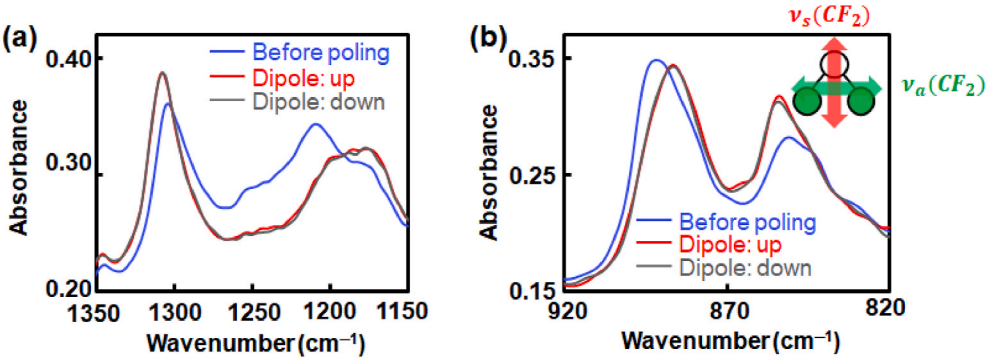

Fig. 3. FT-IR spectra of P(VDF-TrFE) before and after poling treatment in the wavenumber range of (a) 1350−1150 and (b) 920−820 cm^{-1}. Detailed assignment of the peaks can be seen in Table 1. For the spectrum over a wider wavenumber range, see Fig. S2 of Supporting Information. The inset shows the transition moments of the ν_s (CF2) and ν_a (CF2) modes. Green and white balls indicate fluorine and carbon atoms, respectively. (For interpretation of the references to colour in this figure legend, the reader is referred to the Web version of this article.)

film. Therefore, these changes in peak intensity are plausible, as the transition moments of the ν_s (CF_2) mode correspond to the direction of the electric dipole, while that of the ν_a (CF_2) mode is perpendicular to the electric dipole, as shown in the inset of Fig. 3a and b. The higher and lower wavenumber shifts of the ν_s (CF_2) and ν_a (CF_2) peaks are caused by electric-field-induced hardening and softening of molecular vibrations, respectively (for more details, see Fig. S3 in ESI). The other peaks observed at 1201 and 1240 cm^{-1} caused by ν_a (CF_2) absorption of the γ-phase crystal also decreased after poling, which was also attributed to the same orientation changes of the electric dipole. A compositional ratio of 0.66:0.34 for the β-to-γ-phase crystallites within the film before poling was estimated according to a previous report [39]. The spectra of the P(VDF-TrFE) film after poling do not show poling direction (up or down) dependency, exhibiting nearly identical absorbances in all wavenumber ranges, as shown in Fig. 3a and b.

Next, we performed combined measurements of polarization switching and fast time-resolved FT-IR spectroscopy. This evaluation concept has great potential for investigating the molecular dynamics of P(VDF-TrFE) ferroelectricity as it enables simultaneous monitoring of reorientations of electric dipoles and functional groups (transition moments). For this purpose, we used the peak top absorbance of ν_s (CF2) in the β-phase crystal at ~1306 cm^{-1} because its transition moment direction is coincident with that of the electric dipole. A 0.01 Hz triangular electric field was applied to the stacked Al/P(VDF-TrFE)/NiCr device for two cycles, as shown in Fig. 4a. Fig. 4b graphically shows the absorbance and remanent polarization changes induced by this electric field (note that we chased a peak top of ν_s (CF_2) at ~1306 cm^{-1} as it shifts in response to the applied electric field). These peak-top absorbances were used to produce this absorbance plot, and polarization switching was observed during these cycles, as shown in Fig. 4c. The positive and negative remanent polarizations in each cycle were calculated by integrating the corresponding area of the electric current peaks. The coercive electric field is defined as the electric field required for polarization switching (typically the peak top of the electric current in the switching loops).

The first drastic increase in absorbance from 0.362 to 0.385 at 20–30 s is attributed to the dynamic reorientation of electric dipoles in the prepared P(VDF-TrFE) film in the out-of-plane direction (for more details, see Fig. S4 of ESI). This change occurs at an electric field of 75 MV m^{-1}, *i.e.,* 20 MV m^{-1} higher than the coercive electric field (E_c = 55 MV m^{-1} at 115 s in the second cycle). The electric dipoles were randomly oriented in the as-prepared P(VDF-TrFE) film. The initial response of these randomly oriented dipoles to the applied electric field should be slower than that of the once-polarized dipoles. In fact, drastic changes in absorbance occur near the coercive field after the next E_c (−55 MV m^{-1} at 65 s).

Of particular interest here is that the absorbance drops significantly around E_c (−55 and + 55 MV m^{-1} at 65, 115, and 180 s, respectively), and then recovers over E_c. During the polarization reversal process, the transition moment of ν_s (CF_2) must become oriented in the in-plane direction (parallel to the film plane), as shown in Fig. 4d. Therefore, we could simultaneously monitor the dynamics of electric dipole switching and molecular rotations under a *scanning* electric field at the same timeline. This leads us to investigate the polarization switching of P(VDF-TrFE) with high time resolutions, which crucially differs from past reports [40,41]; IR measurements of polarized P(VDF-TrFE) films were performed while applying a *constant* amplitude of electric field or after polarization, because it was technically difficult to detect the absorbance with sufficient time resolutions to determine the fast dynamics of dipole switching.

In Fig. 5a, the second-cycle absorbance near 1306 cm^{-1} associated with ν_s (CF_2) (shown in Fig. 4b (100–200 s)) is replotted so that it is visualized in response to the applied electric field. The electric current density from the Al/P(VDF-TrFE)/NiCr capacitor at each electric field is also shown in the same manner. According to the electric field scan (0 → +100 → 0 → −100 → 0 MV m^{-1}), the electric current density shows a typical switching loop, taking peak tops at an electric field of ±55 MV m^{-1} (defined as coercive electric fields). Meanwhile, the absorbance loop exhibited a clear butterfly-like shape. This type of butterfly-shaped loop is specific to ferroelectric materials, which has also been recognized in the electric-field-dissolved measurements of capacitance [42] and piezoelectric displacement [43] of P(VDF-TrFE). The above-mentioned report on IR measurements under *constant* amplitude of electric field also suggested a similar loop [40,41]; however, the absorbance was not

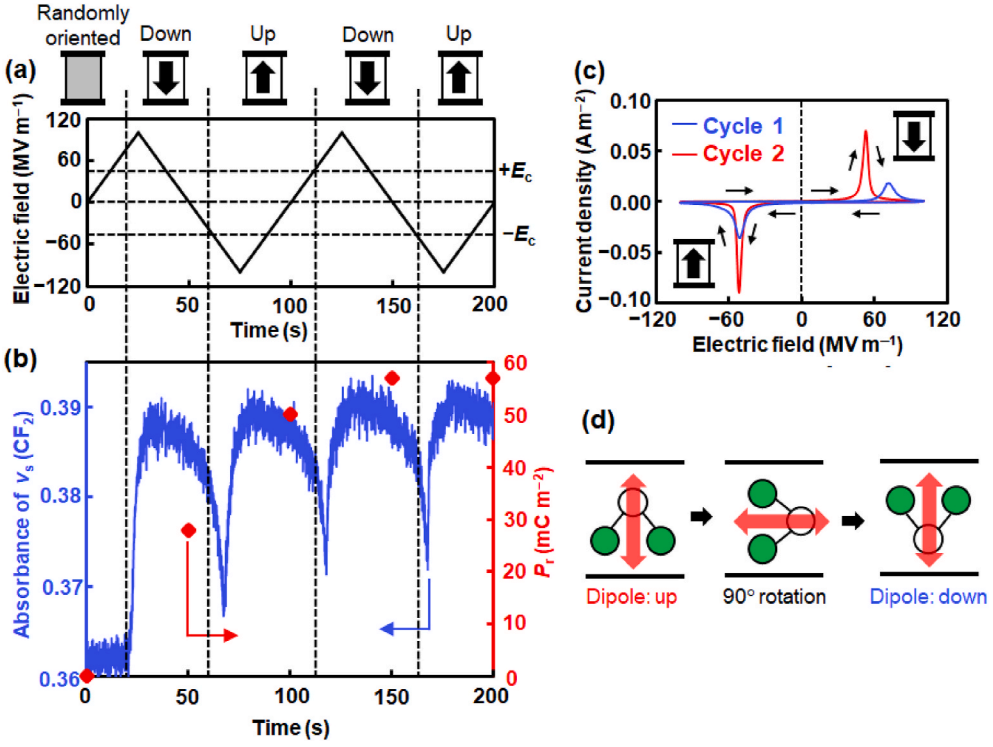

Fig. 4. (a) Time dependence of electric field applied to the P(VDF-TrFE) capacitor. (b) Variations of remanent polarization and absorbance associated with symmetric vibration of CF_2 near 1306 cm^{-1}. Note that the remanent polarization and absorbance are displayed in the same timeline as that shown in panel (a). Moreover, the gradual increase in absorbance by the repeated application of electric field reflects the enhancement of remanent polarization, which is the improvement of dipole alignment in the out-of-plane direction, by repeatedly applying the voltage over the coercive field. (c) Polarization-switching current in response to the applied electric field for 2 cycles. (d) Schematic of molecular rotation during polarization switching. Green and white balls indicate fluorine and carbon atoms, respectively. The transition moment of ν_s(CF2) is depicted by red arrows. Because the RAS technique can detect the transition moment of the molecular vibration aligned in the out-of-plane direction of the film, the absorption of ν_s(CF2) is expected to become minimum when the transition moment rotates for 90° during polarization switching. (For interpretation of the references to colour in this figure legend, the reader is referred to the Web version of this article.)

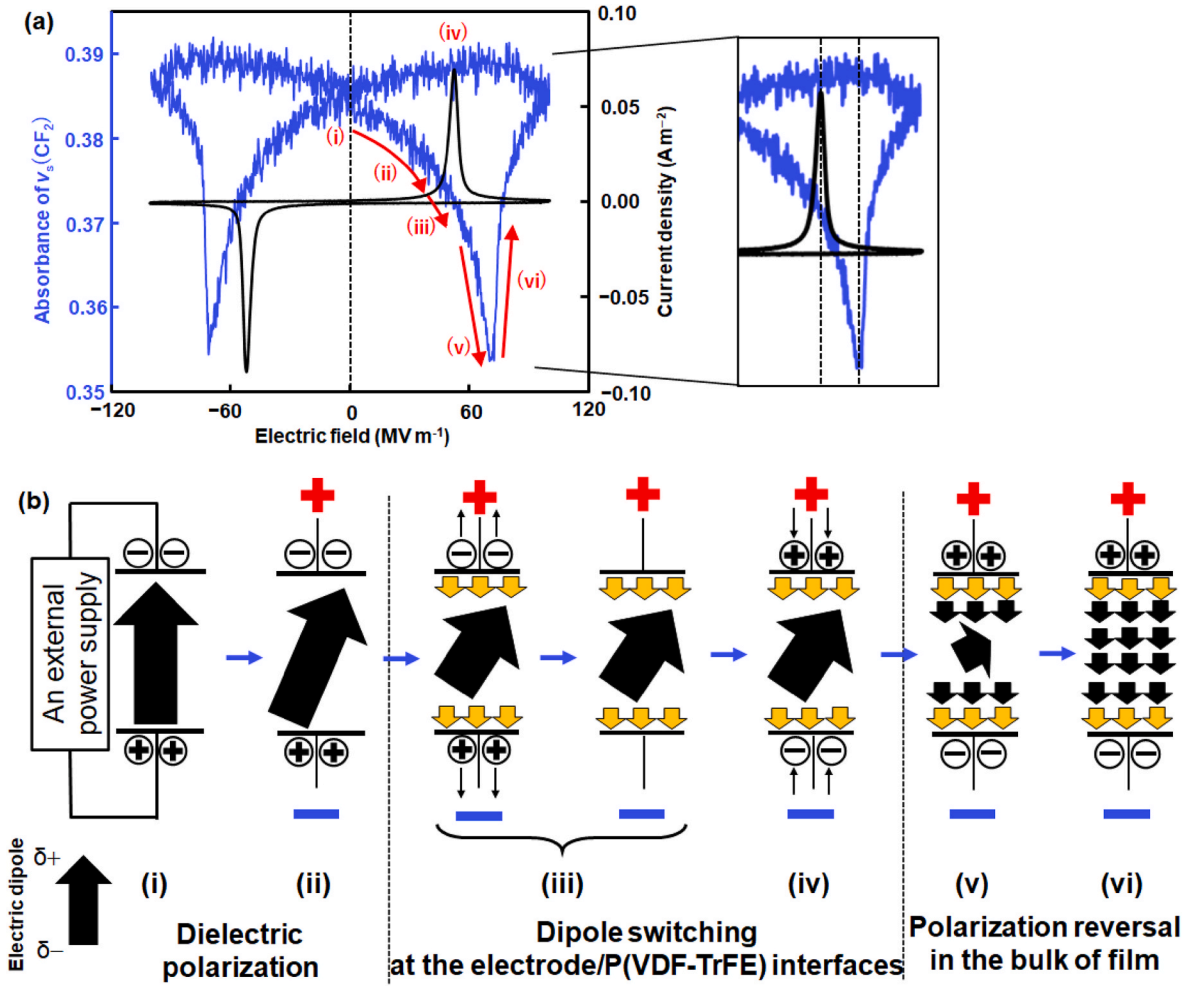

Fig. 5. (a) Polarization switching current and variation of absorbance of ν_s (CF_2) (~1306 cm^{-1}) according to the applied electric field. Note that this graph is produced using the absorbance variation in the second cycle of electric-field scan (at 100–200 s of Figure three) and polarization switching curve shown in Fig. 4c. (b) Schematic of polarization switching dynamics in P(VDF-TrFE) proposed in this study.

simultaneously monitored with the polarization switching curve of current density. In contrast, our measurement concept enables the comparison of (1) the dynamics of electric dipole switching as a function of the electric current loop and (2) functional group (transition moment) rotation as the butterfly-shaped absorbance loop under the same electric field scan in the same timeline.

To compare the electric dipole switching with the transition moment rotation of ν_s (CF_2), we separated the electric field into five regions, as indicated in Fig. 5a. The corresponding electric dipole dynamics are illustrated schematically in Fig. 5b. At stage (i), the electric dipole is in an "up" state at 0 MV m^{-1}. Applying the field in the positive direction gradually decreased the absorbance (stage (ii); 0–50 MV m^{-1}). Because the applied electric field is below $+E_c$ at this stage, this gradual decrease in absorbance is associated with the dielectric polarization that causes weak electric dipole fluctuations. At an electric field of ~50 MV m^{-1}, the electric current density starts to increase (stage (iii)), suggesting a large polarization reversal. The electric current is attributed to the discharge of the capacitor so that the initially accumulated charges in the electrodes start to be released into the external circuit. Importantly, electric dipoles at the interface with the electrodes, not in the bulk of the film, should contribute to the polarization switching at this stage, as illustrated in Fig. 5b. This model was established based on the following reasoning: (1) The absorbance drop at this stage was still gradual, showing a slope similar to that caused by dielectric polarization in stage (ii). This slope was smaller than that observed at the electric field of over $+E_c$ (stage (iv) and (v)); therefore, the number of ν_s (CF_2) transition moments contributing to polarization switching should still be small at stage (iii). (2) The charges of the P(VDF-TrFE) electric dipoles (δ+ and δ–) in the bulk of the film compensate each other or cancel each other out, while the dipoles existing at the interface with electrodes compensate the accumulated charge carriers of the electrodes. The initial discharge of these charge carriers was caused by the switching of the electric dipoles at the interface. Further, external voltages were applied to the dielectric layer and the electrode/dielectric interfaces in the capacitor configuration. Considering that a larger electric field is typically applied to the interface rather than to the bulk of the dielectric layer, the initial electric current at stage (iii) should be caused by the electric dipole switching at the interface.

After the discharging process at stage (iii), charge carriers (with signs opposite to that of the released carriers) reach the electrodes to compensate for the electric dipoles near the electrodes. This charging process was observed as a peak in the electric current density (stage (iv)). The electric field at this peak is generally defined as a coercive field. In the electric field range from 0 to +55 MV m^{-1}, the slope of the absorbance drop was almost the same. In contrast, further application of electric field led to the drastic decrease (stage (v); 50–70 MV m^{-1}) and the subsequent recovery (stage (vi); 70–100 MV m^{-1}) of absorbance. As mentioned above (Fig. 4d), the transition moment of ν_s (CF_2) must become oriented in the in-plane direction (parallel to the film plane) during the polarization reversal process. Because the number of transition moments of ν_s (CF_2) existing in the bulk is much larger than that located at the interface, it is plausible that the drastic drop and recovery

of absorbance at stages (v) and (vi) were mainly caused by the dipole reversal in the bulk. Through these processes, the dipole reorientation from the "up" to the "down" states is completed across the material. It is noteworthy that the drastic drop in absorbance starts at $+E_c$ (from stage (iv) to (v)). After the discharging and charging processes, a large electric field is set up between the two electrodes owing to the newly accumulated charge carriers of the electrodes and the reversed electric dipoles at the interfaces with the electrodes, which stimulates the reversal of electric dipoles in the bulk of the P(VDF-TrFE) film. As shown in Fig. 5b, this process is depicted as the propagation of the polarization switching from the interface to the bulk to make the P(VDF-TrFE) layer "down" polarized step. Similar processes occur when the electric field was applied to the negative side (from the "down" to the "up" poling states) to produce the butterfly-shaped absorbance loop.

In summary, we propose the polarization dynamics of P(VDF-TrFE) as follows: (1) The nucleation of polarization first occurs at the interface between P(VDF-TrFE) and electrodes. (2) Then, the nucleus grows into the bulk of the film to create a completely polarized state across the material.

4. Conclusions

We investigated the polarization reversal mechanism of P(VDF-TrFE) by simultaneously measuring the polarization-switching current and the absorbance variations (molecular orientation changes) of identical capacitors. While P_r strongly reflects the polarization state near the interface between the P(VDF-TrFE) and electrodes, the absorbance is strongly affected by the molecular orientations in the interior of the P(VDF-TrFE) film because the employed RAS method detects all the active transition moments over the entire film. We established a model of polarization switching in the P(VDF-TrFE) film by dividing the polarization-switching current and the butterfly-shaped absorbance variations into six steps against the scanned electric field, which are: (i) initial polarized state, (ii) dielectric response (slight electric dipole alignment or fluctuation) by the applied electric field under E_c, (iii) nucleation of the polarized domain (reversal of ferroelectric dipoles at the interface of P(VDF-TrFE) and electrodes) along with the discharging of the accumulated carriers in the electrode just below E_c, (iv) charging of capacitor to compensate the electric charges of the reversed dipoles at E_c, (v) propagation of the polarized domain toward the interior of the P(VDF-TrFE) film (dipole rotations in the bulk of film), and (vi) complete polarization switching. The obtained results experimentally confirm the conventional Kolmogorov–Avrami–Ishibashi (KAI) model, in which nucleation occurs at the interface between P(VDF-TrFE) and electrodes. The concept described here can be extended to reveal the polarization switching mechanisms of other ferroelectric materials.

Funding

This work was supported in part by JST CREST and JSPS KAKENHI.

CRediT authorship contribution statement

Kohki Uneda: Methodology, Validation, Investigation, Writing – original draft, Visualization. **Shohei Horike:** Writing – review & editing, Visualization. **Yasuko Koshiba:** Methodology, Investigation. **Kenji Ishida:** Conceptualization, Methodology, Supervision.

Declaration of competing interest

The authors declare that they have no known competing financial interests or personal relationships that could have appeared to influence the work reported in this paper.

Acknowledgment

The authors would like to thank JST CREST and JSPS KAKENHI. S.H. would like to thank JST PRESTO.

Appendix A. Supplementary data

Supplementary data to this article can be found online at https://doi.org/10.1016/j.polymer.2022.124822.

References

[1] T. Furukawa, G.E. Johnson, Measurements of ferroelectric switching characteristics in polyvinylidene fluoride, Appl. Phys. Lett. 38 (12) (1981) 1027–1029.
[2] K.M. Ok, E.O. Chi, P.S. Harasyamani, Bulk characterization methods for non-centrosymmetric materials: second harmonic generation, piezoelectricity, pyroelectricity, and ferroelectricity, Chem. Soc. Rev. 35 (8) (2006) 710–717.
[3] R.C.G. Naber, K. Asadi, P.W.M. Blom, D.M. Leeuw, B. Boer, Organic nonvolatile memory devices based on ferroelectricity, Adv. Mater. 22 (9) (2010) 933–945.
[4] D. Pandy, A.P. Singh, V.S. Tiwari, Developments in ferroelectric ceramics for capacitor applications, Bull. Mater. Sci. 15 (5) (1992) 391–402.
[5] S.A. Pullano, I. Mahbub, S.K. Islam, A.S. Fiorillo, PVDF sensor stimulated by infrared radiation for temperature monitoring in microfluidic devices, Sensors 17 (4) (2017).
[6] A.S. Fiorillo, S.A. Pullano, M.G. Bianco, C.D. Critello, Ultrasonic transducers shaped in archimedean and fibonacci spiral: a comparison, sensors 20 (10) (2020).
[7] M. Kang, W. Jung, C. Kang, S. Yoon, Recent progress on PZT based piezoelectric energy harvesting technologies, Actuaters 5 (1) (2016).
[8] E. Rysiakiewicz-pasek, R. Poprawski, J. Polanska, A. Urbanowicz, A. Sieradzki, Properties of porous glasses with embedded ferroelectric materials, J Non Cryst Solids 352 (40–41) (2006) 4309–4314.
[9] Y. Cai, S. Luo, Z. Wang, J. Xiong, H. Gu, Modelling of the electronic and ferroelectric properties of trichloroacetamide using Monte Carlo and first-principles calculations, J Materiomics 3 (2) (2017) 130–134.
[10] T. Yamada, Y. Kudo, N. Kimiduka, Introduction of thiourea into MetalOrganic frameworks by immersion technique and their phase transition characteristics, Chem. Lett. 46 (1) (2017) 115–117.
[11] W.G. Yin, C.G. Duan, W.N. Mei, J. Liu, R.W. Smith, J.R. Hardy, Molecular dynamics simulation of the order-disorder phase transition in solid $NaNO_2$, Phys. Rev. B 68 (17) (2003).
[12] B.D. Mai, H.T. Nguyen, D.Q. Hoang, Influence of cellulose nanoparticles on structure and electrophysical properties of ferroelectrics, Mater. Trans. 60 (12) (2019) 2499–2505.
[13] C. Dagdevirena, B.D. Yanga, Y. Sub, P.L. Tran, P. Joe, E. Anderson, J. Xia, V. Doraiswamy, B. Dehdashti, X. Feng, B. Lu, R. Poston, Z. Khalpey, R. Ghaffari, Y. Huang, M.J. Slepian, J.A. Rogers, Conformal piezoelectric energy harvesting and storage from motions of the heart, lung, and diaphragm, PNAS 111 (5) (2014) 1927–1932.
[14] Y. Kondo, S. Horike, Y. Koshiba, T. Fukushima, K. Ishida, Directly monitoring and power generation from pulsating 3D heart model with organic flexible piezoelectric device, JJAP (2020) 59.
[15] A. Kobayashi, Y. Koshiba, Y. Ueno, T. Kajihara, Y. Tsujiura, M. Morimoto, S. Horike, T. Fukushima, I. Kanno, K. Ishida, Orientation dependence of power generation on piezoelectric energy harvesting using stretched ferroelectric polymer films, JACS (2018) 1052.
[16] A. Salimi, A.A. Yousefi, FTIR studies of β-phase crystal formation in stretched PVDF films, Polym Test 22 (6) (2003) 699–704.
[17] Y. Zheng, J. Zhang, X. Sun, H. Li, Z. Ren, S. Yan, Crystal structure regulation of ferroelectric poly(vinylidene fluoride) via controlled melt-recrystallization, Ind. Eng. Chem. 56 (15) (2017) 4580–4587.
[18] K. Tashiro, in: H.S. Nalwa (Ed.), Crystal Structure and Phase Transition of PVDF and Related Copolymers, Ferroelectric Polymers: Chemistry, Physics, and Applications, Marcel Dekker Inc., 1995, pp. 63–182.
[19] A.J. Lovinger, Recent developments in the structure, properties, and applications of ferroelectric polymers, Appl. Phys 24 (1985) 18–22.
[20] M.M.D. Amos, H.M.G. Correia, S. Lanceros-Méndez, Atomistic modelling of process involved in poling of PVDF, Comput. Maiter. Sci 33 (1–3) (2005) 230–236.
[21] J. Zhang, P. Cao, Z. Cui, Q. Wang, F. Fan, M. Qiu, X. Wang, Z. Wang, Y. Wang, Endowing piezoelectric and anti-fouling properties by directly poling β-phase PVDF membranes with green diluents, AIP Adv 9 (11) (2019).
[22] R. Tanaka, K. Tashiro, M. Kobayashi, Annealing effect on the ferroelectric phase transition behavior and domain structure of vinylidene fluoride (VDF)–trifluoroethylene copolymers: a comparison between uniaxially oriented VDF 73 and 65% copolymers, Polymers 40 (1999) 3855–3865.
[23] T. Feng, D. Xie, Y. Zang, X. Wu, T. Ren, W. Pan, Temperature control of P(VDF-TrFE) copolymer, Thin Films 141 (1) (2013) 187–194.
[24] X. Li, Z. Shi, X. Zhang, X. Meng, Z. Huang, Z. Zhang, The influence mechanism of temperature and storage period on polarization properties of poly (vinylidene fluoride–trifluoroethylene) ultrathin films, Membranes 11 (5) (2021).
[25] S. Miyata, T. Furukawa, *Kyouyuudenntaiporima-* (Ferroelectric Polymer), Kyohritushuppan, Japan, 1988, p. 75 (In Japanese).

[26] R.G. Kepler, R.A. Anderson, Piezoelectricity and pyroelectricity in polyvinylidene fluoride, J. Appl. Phys. 49 (8) (1978) 4490.
[27] A. Roggero, E. Dantras, C. Lacabanne, Poling influence on the mechanical properties and molecular mobility of highly piezoelectric P(VDF-TrFE) copolymer, J Polym Sci B Polym Phys 55 (18) (2017) 1414–1422.
[28] A.C. Choi, A. Pramanic, S.T. Misture, A.R. Paterson, J.L. Jones, O.C. Borkiewicz, Y. Ren, Polarization mechanisms in P(VDF-TrFE) ferroelectric thin films, Phys. Stat. Sol. 12 (10) (2018).
[29] A.J. Bur, J.D. Barnes, K.J. Wahlstrand, A study of thermal depolarization of polyvinylidene fluoride using x-ray pole-figure observations, J. Appl. Phys. 59 (7) (1986) 2345–2354.
[30] Y. Sutani, Y. Koshiba, T. Fukushima, K. Ishida, Formation mechanism of ferroelectric poly (vinylidene fluoride-trifluoroethylene) copolymers with in-plane dipole alignment under low electric field from melt and its SPR based pyroelectric sensor, Polymer (2021) 228.
[31] K. Takashima, Y. Furukawa, Voltage-induced infrared absorption from a spin-cast thin film of ferroelectric poly(vinylidene fluoride-*co*-trifluoroethylene) (P(VDF-TrFE)), Anal Sci 33 (1) (2017) 59–64.
[32] K. Tashiro, H. Yamamoto, S. Kummara, T. Takahama, K. Aoyama, H. Sekiguchi, H. Iwamoto, High-electric-field-induced hierarchical structure change of poly (vinylidene fluoride) as studied by the simultaneous time resolved WAXD/SAXS/FTIR measurements and computer simulations, Macromolecules 54 (5) (2021) 2334–2352.
[33] T. Furukawa, Ferroelectric properties of vinylidene fluoride copolymers, Phase Transitions 18 (3–4) (1989) 143–211.
[34] H. Dvey-Aharon, T.J. Sluckin, P.L. Taylor, Kink propagation as a model for poling in poly(vinylidene fluoride), Phys. Rev. B 21 (8) (1980) 3700–3707.
[35] S. Anwar, K. Asadi, One-dimensional polarization dynamics in ferroelectric polymers, ACS Macro Lett 8 (5) (2019) 525–529.
[36] Y. Sutani, T. Fukushima, A. Mori, Y. Koshiba, T. Kodani, T. Kanemura, K. Ishida, Improvement of thermal stability of an organic pyroelectric infrared sensor with parylene C coating, JJAP 59 (2020).
[37] K. Iida, Y. Imamura, C. Liao, S. Nakamura, G. Sawa, Evaluation of molecular orientation in aromatic polyimide films by FT -IR reflection absorption spectroscopy, Polymer Journal 28 (4) (1996) 352–356.
[38] K.J. Kim, M.N. Reynolds, C. Chang, L.S. Hsu, Spectroscopic analysis of the electric field induced structural changes in vinylidene fluoride/trifluoroethylene copolymer, s. Macromolecules 22 (3) (1989) 1092–1100.
[39] P. Martins, A.C. Lopes, S. L-Mendez, Electroactive phase of poly(vinylidene fluoride): determination, processing and applications, Prog. Polym. Sci. 39 (4) (2014) 683–706.
[40] A. Buchtemann, W. Stark, W. Künstlur, Infrared spectrometric study of poly (vinylidene fluoride) films in cyclic electric fields, Acta Polymerica 42 (4) (1991) 231–237.
[41] H. Isoda, Y. Furukawa, Effect of electric field on the infrared spectrum of a ferroelectric poly(vinylidene fluoride-hexafluoropropylene) film, Vib. Spectrosc. 78 (2015) 12–16.
[42] Y. Miyata, T. Yoshimura, A. Ashida, N. Fujimura, Low-voltage operation of Si-based ferroelectric field effect transistors using organic ferroelectrics, poly (vinylidene fluoride-trifluoroethylene), as a gate dielectric, JJAP 55 (4) (2016).
[43] H. Fang, O. Yan, C. Geng, N.Y. Chan, K. Au, J. Yao, S.M. Ng, C.W. Leung, O. Li, D. Guo, H.L.W. Chan, J. Dai, Facile fabrication of highly ordered poly(vinylidene fluoride-trifluoroethylene) nanodot arrays for organic ferroelectric memory, J. Appl. Phys. 119 (1) (2016).